3D PRINTING

3D nanofabrication by volumetric deposition and controlled shrinkage of patterned scaffolds

Daniel Oran[1]*, Samuel G. Rodriques[1,2]*, Ruixuan Gao[1], Shoh Asano[1,3], Mark A. Skylar-Scott[4,5], Fei Chen[1,6], Paul W. Tillberg[1,7]†, Adam H. Marblestone[1]‡, Edward S. Boyden[1,6,8,9,10]‡§

Lithographic nanofabrication is often limited to successive fabrication of two-dimensional (2D) layers. We present a strategy for the direct assembly of 3D nanomaterials consisting of metals, semiconductors, and biomolecules arranged in virtually any 3D geometry. We used hydrogels as scaffolds for volumetric deposition of materials at defined points in space. We then optically patterned these scaffolds in three dimensions, attached one or more functional materials, and then shrank and dehydrated them in a controlled way to achieve nanoscale feature sizes in a solid substrate. We demonstrate that our process, Implosion Fabrication (ImpFab), can directly write highly conductive, 3D silver nanostructures within an acrylic scaffold via volumetric silver deposition. Using ImpFab, we achieve resolutions in the tens of nanometers and complex, non–self-supporting 3D geometries of interest for optical metamaterials.

Most nanofabrication techniques currently rely on two-dimensional (2D) and 2.5D patterning strategies. Although popular direct laser writing methods allow for the single-step fabrication of self-supporting, polymeric 3D nanostructures (*1*–*8*), arbitrary 3D nanostructures (e.g., solid spheres of metal or metallic wires arranged in discontinuous patterns) are not possible (*9*, *10*). This raises the question of whether a versatile 3D nanofabrication strategy can be developed that would allow independent control over the geometry, feature size, and chemical composition of the final material.

A hallmark of 2D nanofabrication strategies is that materials are deposited in a planar fashion onto a patterned surface. By analogy, we reasoned that a general 3D nanofabrication strategy could involve deposition of materials in a volumetric fashion into a patterned scaffold. However, such scaffolds face a fundamental tension: They should be porous and solvated, to allow for introduction of reagents to their interior, while also being dense, to allow material placement with nanoscale precision. To resolve this contradiction, we reasoned that an ideal scaffold could be patterned in a solvated state and then collapsed and desiccated in a controlled way, densifying the patterned materials to obtain nanoscale feature sizes. Although several groups have experimented with shrinking materials, the shrinking process typically requires harsh conditions and chemical changes that may destroy functional materials (*11*–*13*). We use polyacrylate/polyacrylamide hydrogels for the scaffold material, as they have pore sizes in the range of 10 to 100 nm (*14*), they are known for their ability to expand and shrink up to ~10-fold in linear dimension (*15*–*18*), and methods for optically patterning hydrogels are well established (*19*–*23*).

Our implementation took place in three phases (*24*). It was previously found that two-photon excitation of fluorescein within acrylate hydrogels causes the fluorescein to react with the hydrogel (*21*–*23*). We took advantage of this phenomenon to attach fluorescein molecules carrying reactive groups to the expanded gel in defined 3D patterns (Fig. 1, A and B). In the second phase, after removal of the fluorescein patterning solution, the gel was functionalized by depositing materials onto the patterned reactive groups (Fig. 1, C and D) by using one of several available conjugation chemistries. This volumetric deposition step defines the composition of the material and may be followed by additional deposition chemistries (“intensification”) to boost the functionality of the deposited molecules or nanomaterials (Fig. 1, E and F). Importantly, the functional molecules or nanoparticles are not present during the patterning process, so the specific physical properties of the molecules or nanoparticles used will not affect the patterning. In the final phase, the patterned and functionalized gel scaffold was shrunken by a factor of 10 to 20 in each dimension by using acid or divalent cations over a period of hours, and then it was dehydrated to achieve the desired nanoscale resolution (Fig. 1, G and H). The scaffold was not removed, as it supports the nanofabricated material and allows for the creation of disconnected or high–aspect-ratio structures that would otherwise collapse outside of the scaffold.

We found the polyacrylate gel to be a suitable substrate for patterning and deposition. The gel readily accommodated a wide variety of hydrophilic reagents, including small molecules, biomolecules, semiconductor nanoparticles, and metal nanoparticles (fig. S1, A to C). For laser powers below a critical threshold, the density of the deposited functional material was controllable (Fig. 1I and fig. S2). We estimated, based on the maximum pattern fluorescence (fig. S2A), that binding sites are patterned into the gel at concentrations of at least 79.2 μM in the expanded state, leading to a final concentration in the shrunken state of greater than 272.0 mM, or 1.64×10^{20} sites/cm^3 for a 10× gel (see below). By repeating our patterning and deposition process, we were able to deposit multiple materials in different patterns in the same substrate, such as gold nanoparticles and cadmium telluride nanoparticles (Fig. 1J). We observed by using fluorescence that the deposition of the second material onto the first pattern was at most 18.5% of the deposition of the second material onto the second pattern, confirming that multiple materials may be independently patterned and deposited using this process (fig. S3).

The shrinking process is performed either by exposing the expanded gel to hydrochloric acid or to divalent cations (e.g., magnesium chloride) (fig. S1, A to C). The latter may be useful if the patterned materials are sensitive to acid, although we found that both streptavidin and DNA remained functionally intact after acid shrinking (fig. S1D). Gels that are shrunken in hydrochloric acid can subsequently be dehydrated, resulting in additional shrinking, and this process preserved the patterned geometry (Fig. 1K). The final dehydrated gel was transparent (fig. S4A), and atomic force microscopy (AFM) characterization measured the surface roughness over a 1- by 1-μm window to be ~0.19 nm (root mean square) (fig. S4B). Except where stated otherwise, all samples described as “shrunken” here were shrunken and dehydrated. We tested two different gel formulations that differed only in cross-linker concentration: 10× (0.075% cross-linker) and 20× (0.0172% cross-linker) (*24*). The 10× gels, and the patterns within, shrank consistently by a linear factor of 10.6 ± 0.8 in the lateral dimension (mean ± SD, $n = 5$ gels) and 34.8 ± 1.8 in the axial dimension ($n = 6$ gels) (Fig. 1L), with the disproportionate axial shrink occurring during dehydration, possibly due to surface interactions between the shrinking polymer and the surface of the glass container. For the 20× gels, we observed 20.1 ± 2.9-fold shrink

---

[1] MIT Media Lab, Massachusetts Institute of Technology, Cambridge, MA 02139, USA. [2] Department of Physics, Massachusetts Institute of Technology, Cambridge, MA 02139, USA. [3] Pfizer Internal Medicine Research Unit, Cambridge, MA 02139, USA. [4] John A. Paulson School of Engineering and Applied Sciences, Harvard University, Cambridge, MA 02138, USA. [5] Wyss Institute for Biologically Inspired Engineering, Cambridge, MA 02138, USA. [6] Department of Biological Engineering, Massachusetts Institute of Technology, Cambridge, MA 02139, USA. [7] Department of Electrical Engineering and Computer Science, Massachusetts Institute of Technology, Cambridge, MA 02139, USA. [8] Department of Brain and Cognitive Sciences, Massachusetts Institute of Technology, Cambridge, MA 02139, USA. [9] McGovern Institute, Massachusetts Institute of Technology, Cambridge, MA 02139, USA. [10] Koch Institute, Massachusetts Institute of Technology, Cambridge, MA 02139, USA.

*These authors contributed equally to this work.

†Present address: Janelia Research Campus, Ashburn, VA 20147, USA. ‡These authors contributed equally to this work.

§Corresponding author. Email: esb@media.mit.edu

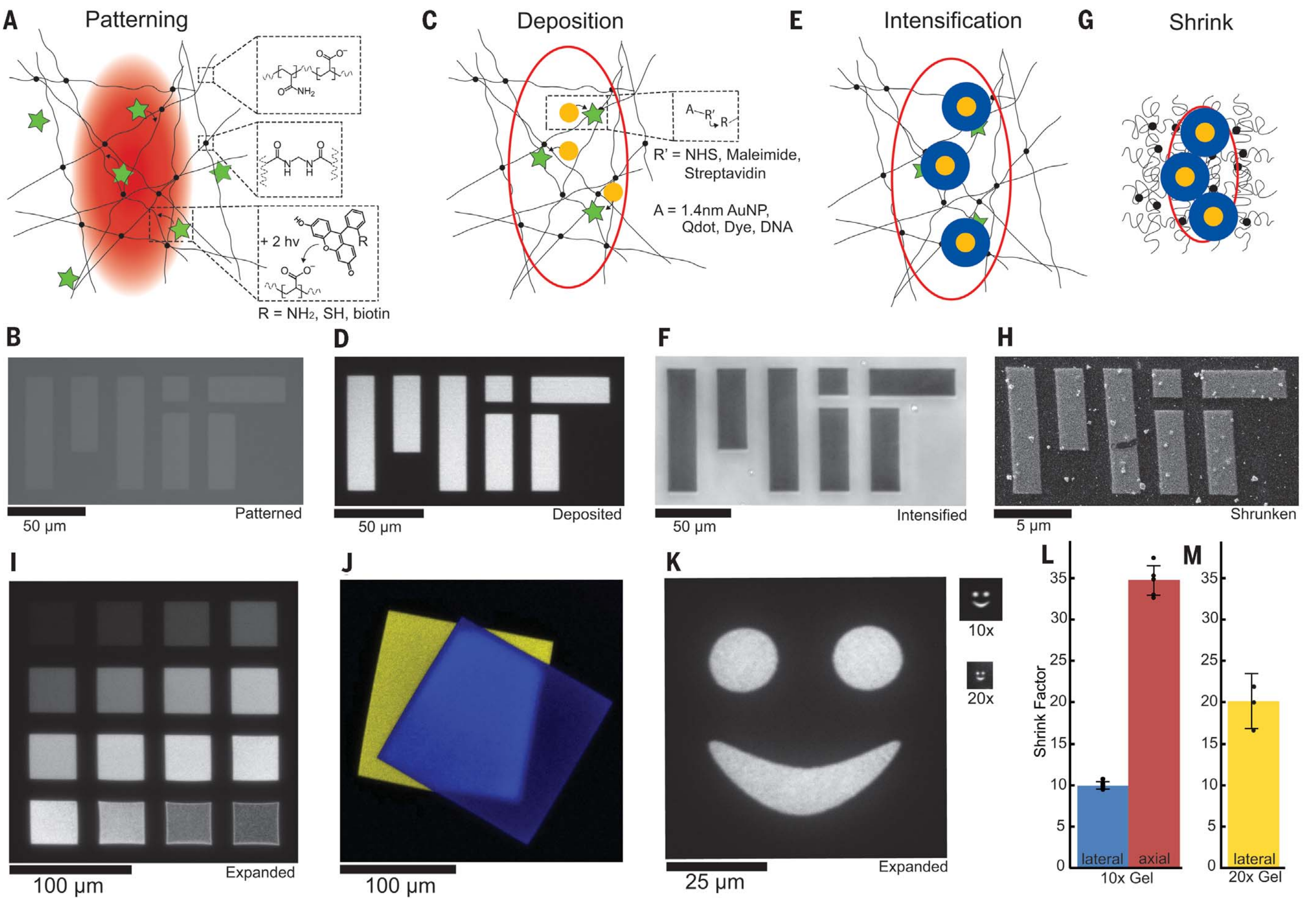

Fig. 1. The ImpFab process. (**A**) Schematic of the patterning process, showing the expanded polyelectrolyte gel (black lines and dots, top insets) and fluorescein (green star, bottom inset) binding covalently to the polymer matrix upon multiphoton excitation (red volume). Not to scale. Fluorescein bears a reactive group, R. h, Planck's constant; ν, frequency. (**B**) Residual fluorescence of patterned fluorescein immediately following patterning. (**C**) Schematic of functionalization of patterned gel by attaching small molecules, proteins, DNA, or nanoparticles to reactive R groups from (A). Red outline indicates patterned volume in (A). (**D**) Image of fluorescent streptavidin nanoparticle conjugates attached to the pattern in (B). (**E**) Schematic of the volumetric deposition process, showing growth of silver (blue) on top of gold nanoparticles within the hydrogel matrix. (**F**) Image of silver deposited onto the pattern in (D) by transmission optical microscopy. Following silver growth, the pattern has high optical density. (**G**) Schematic of the shrinking and dehydration process. (**H**) SEM image of the silverized pattern from (F) following shrinking and dehydration. (**I**) Fluorescent patterns created with different laser powers (*24*). (**J**) Image of a gel patterned with both metal nanoparticles (yellow) and CdTe quantum dots (blue) in different locations. (**K**) Images of fluorescent patterns before shrinking (left, 10× gel), after shrinking and dehydration in a 10× gel (top right) and after shrinking and dehydration in a 20× gel (bottom right). (**L**) The mean lateral (blue) and axial (red) shrink factors (initial size/final size) for 10× gels (n = 6), including dehydration. (**M**) The mean lateral shrink factor for 20× gels (yellow; n = 3). Error bars show SD.

in the lateral dimension (n = 4 gels) (Fig. 1M). The 20× gel formulation is challenging to handle manually due to its delicacy, and so the axial shrink factor was not measured and they were not used further, except for distortion measurements.

To validate the minimum feature size of Implosion Fabrication (ImpFab), we designed a test pattern containing pairs of single-voxel–wide lines (Fig. 2, A to D). Because such postshrink features are necessarily below the optical diffraction limit, we deposited gold nanoparticles and employed scanning electron microscopy (SEM) to assess the resolution after shrinking. We estimated the resolution by measuring the line width [full width at half maximum (FWHM)] (Fig. 2, E to G) and obtained a value of 59.6 ± 3.8 nm (mean ± SD across samples, n = 5) (Fig. 2H) for 10× gels. The mean within-sample standard deviation of the line width was 8.3 nm. We estimated the isotropy of the shrinking process by calculating the ratio of the longest diameter of the patterned circle to the orthogonal diameter (Fig. 2, C and D). The percent distortion thus calculated was 6.8 ± 6.9% for 10× gels (mean ± SD, n = 6 gels) and 8.2 ± 4.3% for 20× gels (n = 4 gels). We found that the ratio of axial to lateral shrink was on average within 3.1 ± 2.5% of the mean of this ratio (n = 6 10× gels), indicating that the disproportionate axial shrink is highly reproducible. Thus, it is possible to account for the disproportionate axial shrink in the design of the pattern. To illustrate this point with the fabrication of a cube, we patterned a rectangular prism and imaged it before and after dehydration (fig. S5). As expected, the rectangular prism contracted in the axial dimension during the dehydration step and turned into a cube.

Because nanoscale metal structures are broadly important in fields such as nanophotonics, metamaterials, and plasmonics, we applied ImpFab to create conductive silver structures. We anchored gold nanoparticles to patterned amines via a biotin-streptavidin linkage (*24*). We were initially unable to deposit gold nanoparticles at high enough concentrations to form conductive structures. We thus developed an intensification process based on photographic intensification chemistries, in which silver was deposited onto the surface of gel-anchored gold nanoparticles in aqueous phase while the gel was in the expanded

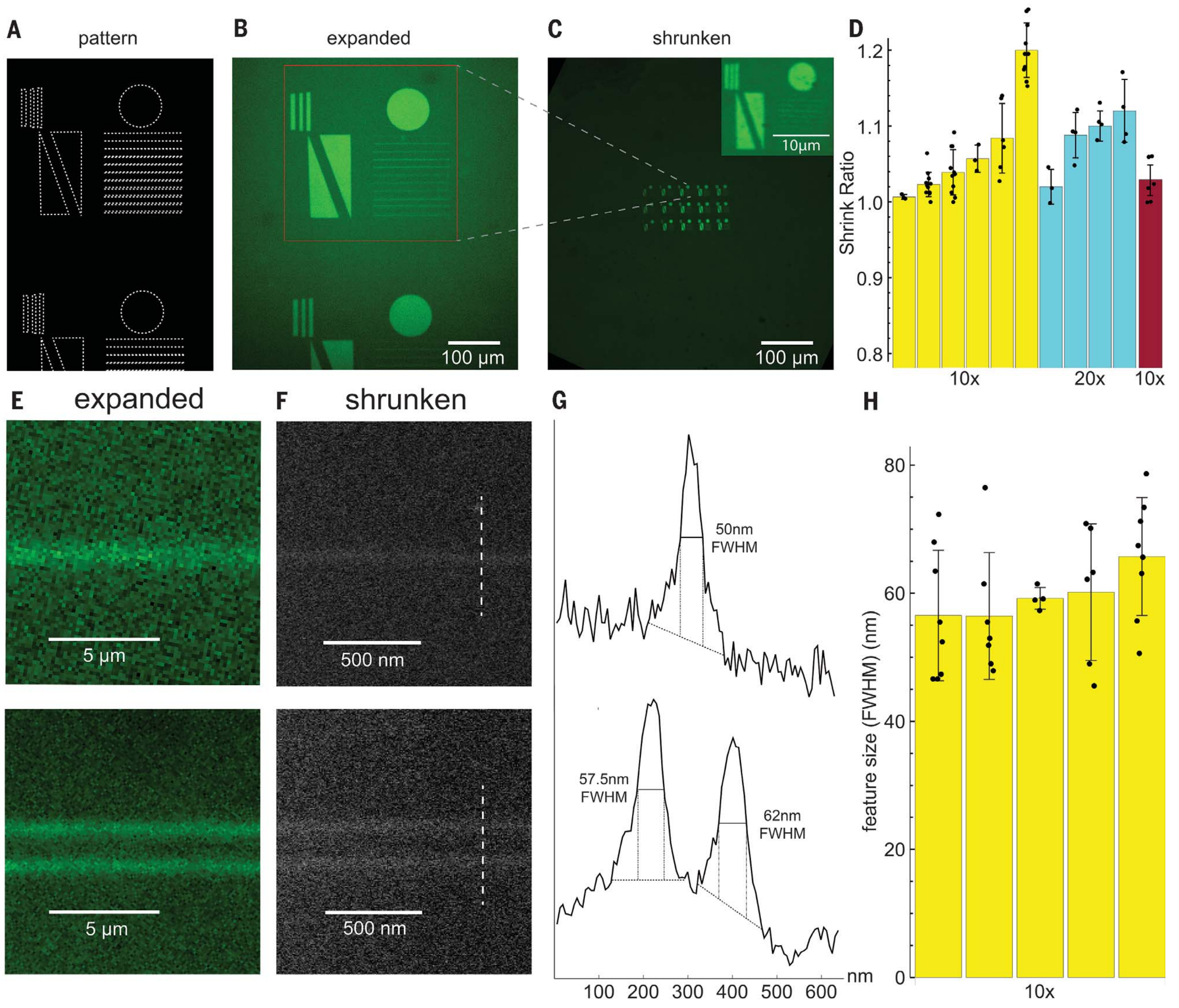

Fig. 2. Resolution of implosion fabrication. (**A**) Design of the resolution test pattern, including pairs of single-voxel-thick lines (bottom right). (**B**) Fluorescence image of the patterns from (A). (**C**) Fluorescence image of the pattern from (B) after shrinking. (**D**) Measures of isotropy in lateral and axial dimensions. Yellow and blue bars represent lateral isotropy for 10× gels and 20× gels, respectively, and the red bar represents axial isotropy for 10× gels. (**E**) Fluorescence images of single-voxel lines before shrinking. (**F**) SEM images of single-voxel lines after 10× shrinking. The gel was functionalized with gold nanoparticles for contrast. (**G**) Cross-sectional intensity profiles of the lines imaged by SEM [dashed lines in (F)], showing how the FWHM of single voxel lines were measured. (**H**) Line widths, measured in (G), for five different gel samples. Dots are measurements for individual lines; bars indicate means ± SD, across individual lines within a single gel.

state (Fig. 1, E and F). Finally, the gel was treated with a chelating agent to remove any remaining dissolved silver and was then shrunken via exposure to hydrochloric acid and subsequent dehydration.

Even with the silver intensification process, wire structures fabricated using the method above (Fig. 3A) were not reliably conductive, or they had resistances on the order of hundreds of ohms. We tested several different methods of sintering, including treatment with oxygen plasma, electrical discharge, and heating the sample to ~500°C in an oven. However, none of these methods resulted in well-preserved and evenly sintered silver structures. Instead, we found that the silver patterns could be sintered effectively when we used the same two-photon setup used for the initial photopatterning step. We found that samples irradiated at relatively low power levels (*24*) showed a distinct change in the morphology of the embedded silver nanoparticles that was consistent with sintering (Fig. 3, B and C). We measured the conductivity of three patterned silver squares both before and after sintering and found that the resistance of each square decreased by 20- to 200-fold (Fig. 3D). Sintered wires were measured in a four-point probe system and were found to have linear IV curves (fig. S6A). Wires sintered in this way had an average resistance of 2.85 ± 1.68 ohms (mean ± SD, n = 10), with the resistance depending on the density of the patterned silver (fig. S6B). By contrast, an ideal silver wire with the same geometry would have a resistance of 0.38 ohms, suggesting that our sintered structures achieved a mean conductivity 13.3% that of bulk silver, with individual samples obtaining conductivities as high as 30% that of bulk silver (Fig. 3E).

To verify that our method is compatible with a wide range of 3D geometries, we fabricated structures with dimensions ranging from hundreds of nanometers to several micrometers (Fig. 4, A to C). We found that these structures retained their morphology following sintering (Fig. 4B). We fabricated a nonlayered, nonconnected 3D structure comprised of many 2D substructures arranged at different angles relative to each other in space, which would not lend itself to fabrication by other means (Fig. 4D). Whereas our previous experiments had only observed the fabrication of 2D silver structures, we used confocal reflection microscopy to confirm that silver was deposited throughout the volume of the 3D pattern (Fig. 4E). Finally, using confocal microscopy, we were able to validate that the structure retained its shape after shrinking (Fig. 4F).

Due to the modular nature of ImpFab, the extension of the ImpFab strategy to other kinds of materials, such as other semiconductors or metals, only requires the development of an aqueous deposition chemistry that is compatible

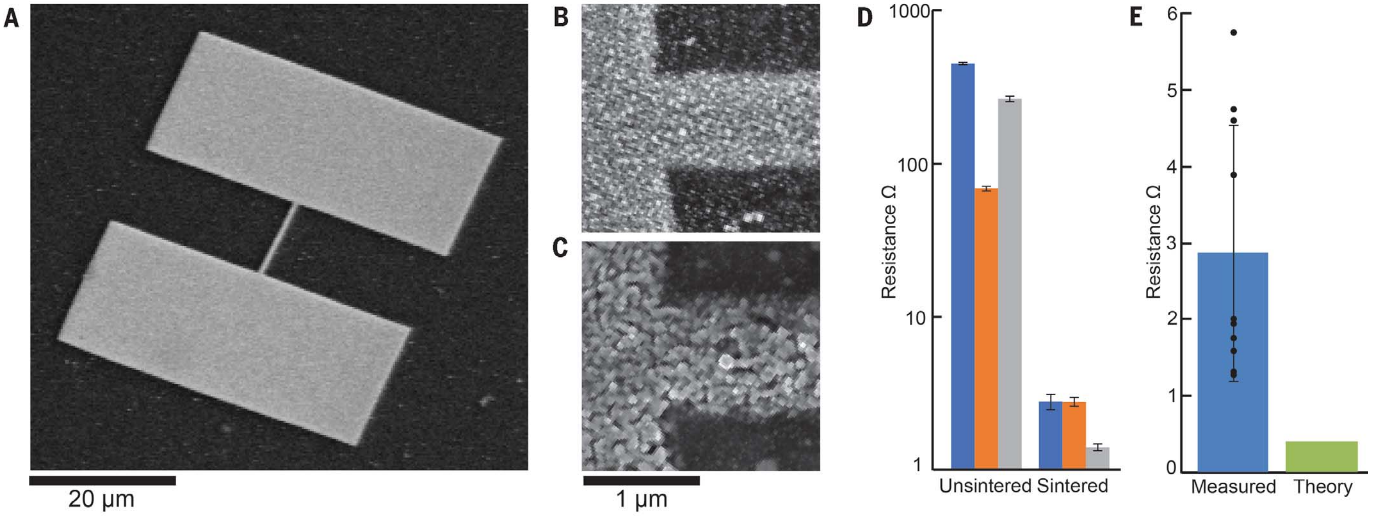

Fig. 3. Characterization of silver conductivity. (**A**) SEM overview of a shrunken silver wire between two landing pads, prior to sintering. (**B** and **C**) SEM images of wires before (B) and after (C) sintering. (**D**) Resistance of three separate conductive pads, each with dimensions of 35 μm by 35 μm, measured before and after sintering. Each color represents a single conductive pad. Error bars show standard errors in a four-point conductivity measurement. (**E**) Resistance of individual sintered wires (black dots) and the means (blue) and standard deviations, compared to the theoretical conductivity of a similar structure made of bulk silver (green).

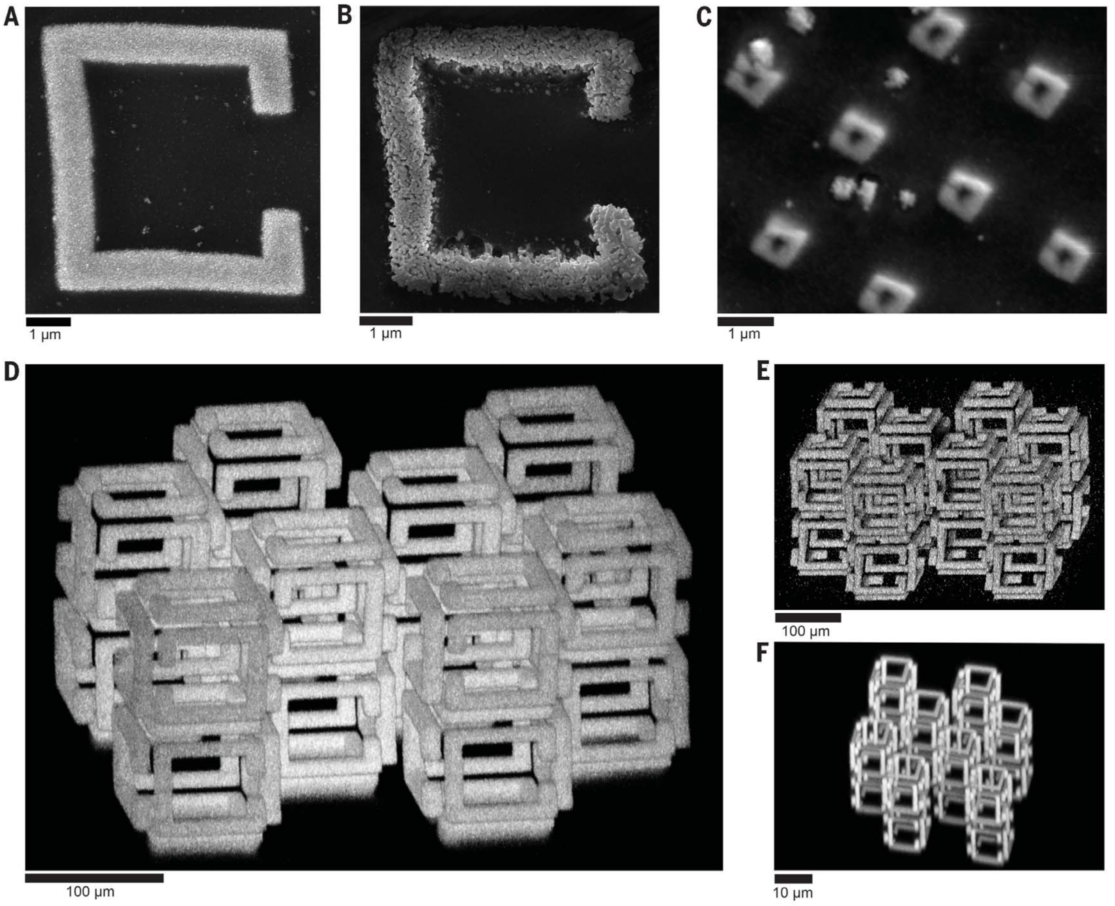

Fig. 4. Fabrication of 3D metal nanostructures. (**A** and **B**) 2D structures fabricated with ImpFab with micrometer-scale resolution, before (A) and after (B) sintering (visualized via SEM). (**C**) Similar structures fabricated with a 100-nm feature size, after shrinking and dehydration but before sintering. (**D**) Maximum-intensity projection of a fluorescent image of a 3D structure before shrinking (*2*, *28*). (**E**) Maximum-intensity projection of a reflected light image from the same structure following volumetric silver deposition, prior to shrinking. (**F**) Maximum-intensity projection of a fluorescent image of the same structure shrunken but not dehydrated.

with the gel substrate. Future iterations may use alternative chemistries, such as dendrimeric complexes for direct deposition of metals or semiconductors within the hydrogel (*25*, *26*), or DNA-addressed material deposition (*27*). Finally, we note that although we used a conventional microscope that was not optimized for patterning and that was limited to a 4-cm/s scan speed (in postshrink dimensions), we were able to create objects spanning hundreds of microns to millimeters (fig. S7). With the use of faster patterning systems (*23*), ImpFab could ultimately enable the creation of centimeter-scale nanomaterials.

REFERENCES AND NOTES

1. M. Deubel *et al*., *Nat. Mater.* **3**, 444–447 (2004).
2. C. M. Soukoulis, M. Wegener, *Nat. Photonics* **5**, 523–530 (2011).
3. C. A. Ross, K. K. Berggren, J. Y. Cheng, Y. S. Jung, J.-B. Chang, *Adv. Mater.* **26**, 4386–4396 (2014).
4. J.-B. Chang *et al*., *Nat. Commun.* **5**, 3305 (2014).
5. I. Wathuthanthri, Y. Liu, K. Du, W. Xu, C.-H. Choi, *Adv. Funct. Mater.* **23**, 608–618 (2013).
6. S. Matsui, T. Kaito, J. Fujita, M. Komuro, K. Kanda, *J. Vac. Sci. Technol. B* **3181**, 3–7 (2000).
7. S. Kawata, H. B. Sun, T. Tanaka, K. Takada, *Nature* **412**, 697–698 (2001).
8. L. R. Meza, S. Das, J. R. Greer, *Science* **345**, 1322–1326 (2014).
9. A. Vyatskikh *et al*., *Nat. Commun.* **9**, 593 (2018).
10. Y. Y. Cao, N. Takeyasu, T. Tanaka, X. M. Duan, S. Kawata, *Small* **5**, 1144–1148 (2009).
11. J. Bauer, A. Schroer, R. Schwaiger, O. Kraft, *Nat. Mater.* **15**, 438–443 (2016).
12. M. Hegde *et al*., *Adv. Mater.* **29**, 1701240 (2017).
13. X.-M. Zhao, Y. Xia, O. J. A. Schueller, D. Qin, G. M. Whitesides, *Sens. Actuators A Phys.* **65**, 209–217 (1998).
14. D. L. Holmes, N. C. Stellwagen, *Electrophoresis* **12**, 612–619 (1991).
15. F. Chen, P. W. Tillberg, E. S. Boyden, *Science* **347**, 543–548 (2015).
16. F. Ilmain, T. Tanaka, E. Kokufuta, *Nature* **349**, 400–401 (1991).
17. Y. Hirokawa, T. Tanaka, *AIP Conf. Proc.* **107**, 203–208 (1984).
18. A. Suzuki, T. Tanaka, *Nature* **346**, 345–347 (1990).
19. C. A. DeForest, K. S. Anseth, *Nat. Chem.* **3**, 925–931 (2011).
20. C. A. DeForest, K. S. Anseth, *Angew. Chem.* **124**, 1852–1855 (2012).
21. M. A. Skylar-Scott, M.-C. Liu, Y. Wu, M. F. Yanik, in *Proc. SPIE 10115, Advanced Fabrication Technologies for Micro/Nano Optics and Photonics X* (International Society for Optics and Photonics, 2017), abstr. 101150L.
22. M. A. Skylar-Scott, M.-C. Liu, Y. Wu, A. Dixit, M. F. Yanik, *Adv. Healthc. Mater.* **5**, 1233–1243 (2016).
23. M. A. Scott, Z. D. Wissner-Gross, M. F. Yanik, *Lab Chip* **12**, 2265–2276 (2012).
24. Materials and methods are available as supplementary materials.
25. A. Miura *et al*., *Opt. Mater. Express* **7**, 2224 (2017).
26. K. Esumi, A. Suzuki, N. Aihara, K. Usui, K. Torigoe, *Langmuir* **14**, 3157–3159 (1998).
27. P. W. K. Rothemund, *Nature* **440**, 297–302 (2006).
28. D. B. Burckel *et al*., *Adv. Mater.* **22**, 5053–5057 (2010).

ACKNOWLEDGMENTS

We thank, for helpful discussions, T. Swager, M. Soljacic, J. Bewersdorf, I. Gupta, and N. Barry. We also thank W. Salmon, N. Watson, N. Savidis, S. Terclavers, S. E. Kooi, E. B. Kromann, and M. Lessard for useful suggestions and technical assistance with imaging. We thank the anonymous referees for helpful comments that improved the manuscript. **Funding:** E.S.B. acknowledges funding by the Kavli Dream Team program, the HHMI-Simons Faculty Scholars Program, the Open Philanthropy Project, John Doerr, ONR N00014-17-1-2977, NIH 1R01EB024261, NIH 1U01MH106011, the New York Stem Cell Foundation-Robertson Award, NIH Director's Pioneer Award 1DP1NS087724, the U.S. Army Research Laboratory and the U.S. Army Research Office under contract number W911NF1510548, NIH 1R01MH103910, NIH 2R01DA029639, the MIT Media Lab, NIH 1RM1HG008525, and NIH 1R24MH106075. S.G.R. acknowledges funding through the Hertz Graduate Fellowship and the National Science Foundation Graduate Research Fellowship Program (award 1122374). **Author contributions:** S.G.R., D.O., M.A.S.-S., F.C., P.W.T., A.H.M., and E.S.B. conceived of strategies for implosion fabrication. S.G.R. and D.O. conceived of and developed the implosion fabrication gel, patterning, deposition, intensification, and shrink chemistries. S.G.R., D.O., R.G., A.H.M., and E.S.B. conceived of validation strategies. R.G. performed imaging for the results shown in Fig. 2F and fig. S4. S.A. wrote the program for generating arbitrary 3D patterns using the Zen software. S.G.R., D.O., A.H.M., and E.S.B. wrote the paper, with contributions and edits from all authors. **Competing interests:** S.G.R., D.O., S.A., R.G., F.C., P.W.T., A.H.M., M.A.S.-S., and E.S.B. are inventors on a patent filed on implosion fabrication. A.H.M. is also affiliated with Deepmind Technologies Ltd. F.C. is also affiliated with the Broad Institute of Harvard and MIT. **Data and materials availability:** Analyzed image data used to produce Fig. 1L and Fig. 2D (red bar) are provided as CSV files in the supplementary materials. Conductivity data used to produce Fig. 3, D and E, and fig. S6 are provided as CSV files in the supplementary materials. Raw image data used to produce fig. S2 and Fig. 2D (yellow and blue bars) and Fig. 2, G and H, are provided in the supplementary materials.

SUPPLEMENTARY MATERIALS

www.sciencemag.org/content/362/6420/1281/suppl/DC1
Materials and Methods
Figs. S1 to S7
Tables S1 to S3
Data S1

18 June 2018; accepted 2 November 2018
10.1126/science.aau5119

Science

3D nanofabrication by volumetric deposition and controlled shrinkage of patterned scaffolds

Daniel Oran, Samuel G. Rodriques, Ruixuan Gao, Shoh Asano, Mark A. Skylar-Scott, Fei Chen, Paul W. Tillberg, Adam H. Marblestone and Edward S. Boyden

Science **362** (6420), 1281-1285.
DOI: 10.1126/science.aau5119

Shrinking problems in 3D printing

Although a range of materials can now be fabricated using additive manufacturing techniques, these usually involve assembly of a series of stacked layers, which restricts three-dimensional (3D) geometry. Oran *et al.* developed a method to print a range of materials, including metals and semiconductors, inside a gel scaffold (see the Perspective by Long and Williams). When the hydrogels were dehydrated, they shrunk 10-fold, which pushed the feature sizes down to the nanoscale.

Science, this issue p. 1281; see also p. 1244

ARTICLE TOOLS	http://science.sciencemag.org/content/362/6420/1281
SUPPLEMENTARY MATERIALS	http://science.sciencemag.org/content/suppl/2018/12/12/362.6420.1281.DC1
RELATED CONTENT	http://science.sciencemag.org/content/sci/362/6420/1244.full
REFERENCES	This article cites 26 articles, 2 of which you can access for free http://science.sciencemag.org/content/362/6420/1281#BIBL
PERMISSIONS	http://www.sciencemag.org/help/reprints-and-permissions

---

Science (print ISSN 0036-8075; online ISSN 1095-9203) is published by the American Association for the Advancement of Science, 1200 New York Avenue NW, Washington, DC 20005.